Measured Unsteady Transonic Aerodynamic Characteristics of an Elastic Supercritical Wing

David A. Seidel,* Maynard C. Sandford,† and Clinton V. Eckstrom‡
NASA Langley Research Center, Hampton, Virginia

Transonic steady and unsteady aerodynamic data were measured on a large elastic wing in the NASA Langley Transonic Dynamics Tunnel. The wing had a supercritical airfoil shape and a leading-edge sweepback of 28.8 deg. The wing was heavily instrumented to measure both static and dynamic pressures and deflections. A hydraulically driven outboard control surface was oscillated to generate unsteady airloads on the wing. Representative results from the wind-tunnel tests are presented and discussed. An experimentally predicted dynamic wing instability boundary, sensitive to angle of attack, is reported.

Nomenclature

C_p = pressure coefficient
f = frequency of oscillating control surface, Hz
M = freestream Mach number
q = freestream dynamic pressure, psf
x/c = chordwise location, fraction of local chord
α = wing root angle of attack, deg (positive leading edge up)
δ_d = amplitude of control surface oscillation, deg
δ_m = mean control surface deflection angle, deg (positive leading edge up)
ΔC_p = lifting pressure coefficient (positive up)
η = spanwise location, fraction of semispan

Introduction

FOR the past decade, the NASA Langley Research Center has pursued a program of unsteady pressure measurements on essentially rigid wing models for the purpose of evaluating computational transonic aerodynamic codes, and three such models have been tested in the Transonic Dynamics Tunnel (TDT). These rigid large-wing configurations included a clipped delta wing with a circular arc airfoil,[1] a high-aspect-ratio wing with a supercritical airfoil,[2] and a rectangular wing with a supercritical airfoil.[3] All these wings were made rigid to minimize dynamic structural effects and thereby simplify correlation with the computational results. Real airplane wings are elastic structures, however, and it is desirable to test an elastic wing model to assess the accuracy of transonic computer codes for predicting the aeroelastic response of wings, including flutter.

A delay in the NASA program Drones for Aerodynamic and Structural Testing (DAST)[4] made the second Aeroelastic Research Wing, ARW-2, available for testing in the Langley TDT. This elastic-wing configuration had an aspect ratio of 10.3, a leading-edge sweepback angle of 28.8 deg, and a supercritical airfoil. The wing had a hydraulically driven outboard trailing-edge control surface and was instrumented with unsteady pressure gages. The primary purpose of these tests was to obtain unsteady pressure measurements on an elastic wing. Secondary objectives were to provide an early assessment of the wing aeroelastic stability over a wide range of angles of attack and to provide wind-tunnel data for comparison with planned flight test data.

This paper presents some representative results from the elastic wing tests in which the outboard control surface was used to generate unsteady pressures. Wind-tunnel Mach numbers varied from 0.60 to 0.90 at dynamic pressures from less than 50 to over 300 psf. Model parameters investigated include wing angle of attack, control surface mean angle, and control surface oscillation amplitude and frequency.

Wind-Tunnel Model

General

The elastic semispan wing used in the present study is the DAST ARW-2 right-wing panel. A half-body fuselage was used to simulate the drone fuselage. This fuselage had shorter nose and tail sections than the drone fuselage since no supersonic tests were to be made. The center section of the fuselage was similar to the actual drone fuselage in both diameter and wing location to generate the proper airflow over the inboard section of the wing. Both the fuselage and the wing were mounted on a remotely controlled turntable mechanism located on the tunnel sidewall. Figure 1 shows the wing and fuselage configuration mounted in the wind tunnel.

The ARW-2 was designed structurally, using an integrated design procedure, to utilize active control systems for maneuver load alleviation, gust load alleviation and flutter suppression.[4] The wing structure is described in Ref. 5. The wing primary structure consisted of a front spar at 25% of local chord and a rear spar at 62% of local chord. Ribs were placed perpendicular to the rear spar every 13.2 in. except for the outboard wing-tip rib, which also served as a spar end fitting. The spars and ribs were machined from 7075-T73 aluminum alloy. The wing skin was made of fiberglass material with honeycomb panels sandwiched between the middle two layers of fiberglass for areas of skin not located over the spars or ribs. The number of layers of fiberglass used to make the skin varied from 36 at the inboard end to 27 at the outboard end, with approximately 25% of the layers at ±45-deg orientation.

Received April 11, 1985; presented as Paper 85-0598 at the AIAA/ASME/ASCE/AHS 26th Structures, Structural Dynamics and Materials Conference, April 15-17, 1985; revision received Jan. 22, 1987.

*Aerospace Engineer, Unsteady Aerodynamics Branch, Loads and Aeroelasticity Division. Member AIAA.
†Aerospace Engineer, Configuration Aeroelasticity Branch, Loads and Aeroelasticity Division. Member AIAA.
‡Aerospace Engineer, Aeroservoelasticity Branch, Loads and Aeroelasticity Division. Member AIAA.

Geometry

The wing planform and instrumentation locations are shown in Fig. 2. The wing had an aspect ratio of 10.3, with a leading-edge sweep angle of 28.8 deg. The wing was equipped with three hydraulically driven control surfaces, two inboard and one outboard. The inboard surfaces were held fixed at 0-deg deflection, and only the outboard surface was deflected statically and dynamically. The outboard surface hinge line was located at 77% of local chord.

The wing contour was formed from three different supercritical airfoils. These three airfoils were located at the following spanwise wing stations: the wing-fuselage junction ($\eta = 0.071$), the wing planform break ($\eta = 0.426$), and the wing tip ($\eta = 1.000$), and had thickness-to-chord ratios of 0.15, 0.12, and 0.11, respectively. The three supercritical airfoil shapes and wing twist were defined for the design cruise condition and are described in Ref. 6. Straight-line interpolation along constant-percent chords was used to define the wing contour between these three airfoil sections. The wing construction jig shape was then derived from the defined cruise shape, the corresponding loading conditions, and the flexibility of the wing structure.

Instrumentation

The locations of the wing instrumentation are shown in Fig. 2. The instrumentation consisted of 191 pressure transducers and 10 accelerometers. In addition, strain gages were located near the wing root to measure bending moments. Differential pressure gages were mounted in each supply line to the hydraulic actuators of each control surface to measure hinge moments. Small potentiometers were used to measure the control surface angular displacement. The model angle of attack was measured by a servo accelerometer that was mounted near the wing root. Both steady and unsteady pressures were obtained using differential pressure transducers referenced to the tunnel's static pressure. Streamwise rows of upper and lower surface pressure orifices were located at six span stations. The orifice rows were located at $\eta = 0.274$, 0.476, 0.599, 0.707, 0.871, and 0.972. The fifth row at $\eta = 0.871$ lies along the midspan of the outboard control surface. All these surface orifices were connected to pressure transducers by matched tubes having a 0.040-in. i.d. and a length of 18 in. In order to determine the tube transfer functions needed to correct the unsteady pressure data from these matched-tube transducers, simultaneous measurements were also obtained from a row of *in situ* transducers mounted on the wing upper surface parallel to the fifth row of surface orifices. Dynamic wing deflections were determined using the 10 accelerometers.

Wind Tunnel

The Langley Transonic Dynamics Tunnel (TDT) is a closed-circuit continuous-flow tunnel, which has a 16-ft square test section with slots in all four walls. Mach number and dynamic pressure can be varied simultaneously, or independently, with either air or Freon as a test medium. Freon was used for the majority of tests in the investigation.

Data Acquisition and Analysis

Data from the model instrumentation were acquired using the TDT real-time data-acquisition system.[7] The pressure data were acquired using the electronically scanned pressure (ESP) system.[8] The ESP system is a sequential, digital pressure-sampling system equivalent to a mechanical scanivalve. All data were digitized in real time at 250 sample/s and written on magnetic tape for later analysis. Static pressures were measured by all 191 pressure transducers. Each pressure signal was averaged for 1.2 s to acquire its mean value.

Dynamic pressure time histories for the three outboard rows of surface orifices and accelerometer time histories were recorded for a minimum of 50 cycles of control surface oscillation. Discrete Fourier transforms of these time histories then provided the magnitude and phase angle at the frequency of the oscillating control surface for each transducer and accelerometer. All phase angles are relative to the position of the oscillating control surface.

Wing bending moments were measured for all cases in which static pressures were recorded. The bending gage measurements were averaged for 0.3 s to obtain a mean value for wing bending moment for each gage.

The control surface static hinge moments were measured using two pressure gages installed in each of the two hydraulic supply lines to the actuator.[2] The mean value of the differential pressure between the two gages is directly related to the control surface hinge moment. To obtain quasi-steady hinge moments, the control surface was oscillated at a low frequency of 0.5 Hz and amplitude δ_d of 1 deg to eliminate the influence of high friction loads created by the internal seal of the actuator. The resulting differential signal was averaged for 10 s to acquire a mean value for the hinge moment.

Test Results and Discussion

Steady and unsteady pressures were measured for a large number of test conditions in the TDT, using Freon as a test medium. The test conditions at which pressure data were taken is shown in Fig. 3. Data were taken at Mach numbers of 0.6, 0.7, 0.8, 0.85, and 0.88 and at dynamic pressures of 100, 200, and 300 psf. At each tunnel condition, static pressure data were taken for wing angles of attack of -2 to 4 deg for the control surface undeflected ($\delta_m = 0$ deg). Some of the high-angle-of-attack values were eliminated at the higher dynamic pressures owing to maximum bending moment restrictions imposed on the wing. For wing angles of attack of 0 and 2 deg, the control surface static deflection δ_m was varied from -8 to 8 deg. Unsteady pressure data were taken at wing angles of attack of 0 and 2 deg for control surface oscillation amplitudes

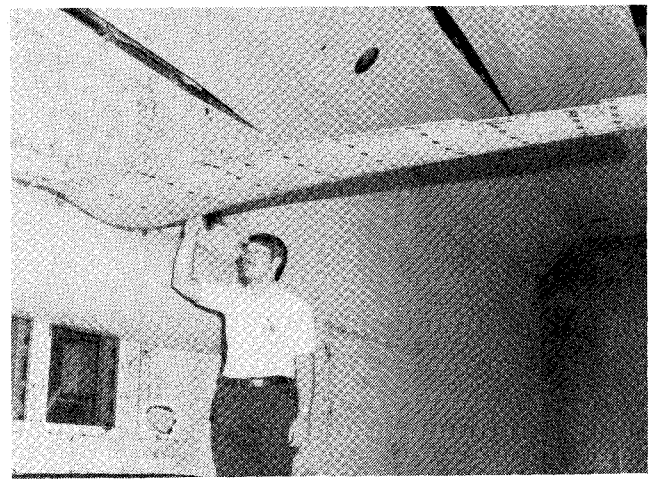

Fig. 1 Wing mounted in TDT test section.

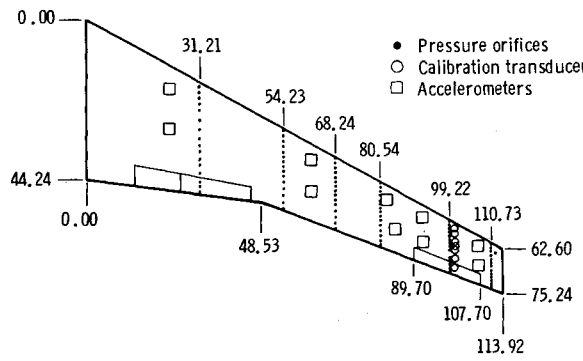

Fig. 2 Wing planform and instrumentation locations (in.).

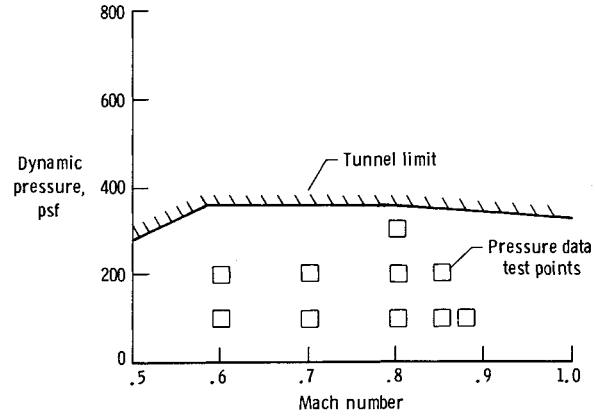

Fig. 3 Wind-tunnel test conditions.

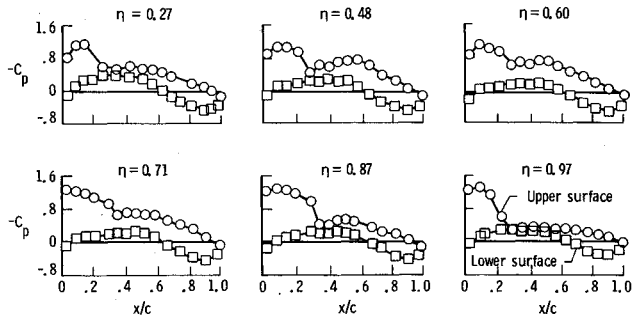

Fig. 4 Steady chordwise pressure distributions at six span stations; $M=0.80$, $\alpha=2$ deg, $q=100$ psf, and $\delta_m=0$ deg.

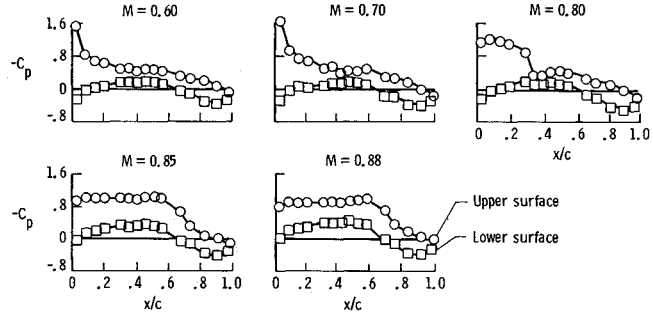

Fig. 5 Steady chordwise pressure distributions for five Mach numbers at $\eta=0.87$; $\alpha=2$ deg, $q=100$ psf, and $\delta_m=0$ deg.

of δ_d equal to 1, 2, and 3 deg and frequencies of 5, 15, and 20 Hz.

Steady Pressure Results

Span Effects

Figure 4 shows the steady chordwise pressure distribution at the six span stations near the design cruise condition ($M=0.8$, $\alpha=2$ deg, $q=100$ psf, and $\delta_m=0$ deg). The data show that a shock is present on the upper surface of the wing and that the shock location varies with span. The steady shock location, in terms of local chord, moves aft between 27 and 87% span, then moves forward between 87 and 97% span.

Mach Number Effects

Figure 5 shows the steady pressure distributions at the 87% span station for five Mach numbers for 2-deg angle of attack, a dynamic pressure of 100 psf, and an outboard mean control

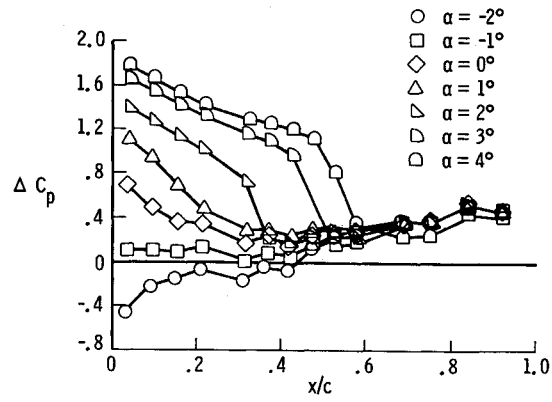

Fig. 6 Effect of angle of attack on steady lifting pressure distribution at $\eta=0.87$; $M=0.80$, $q=100$ psf, and $\delta_m=0$ deg.

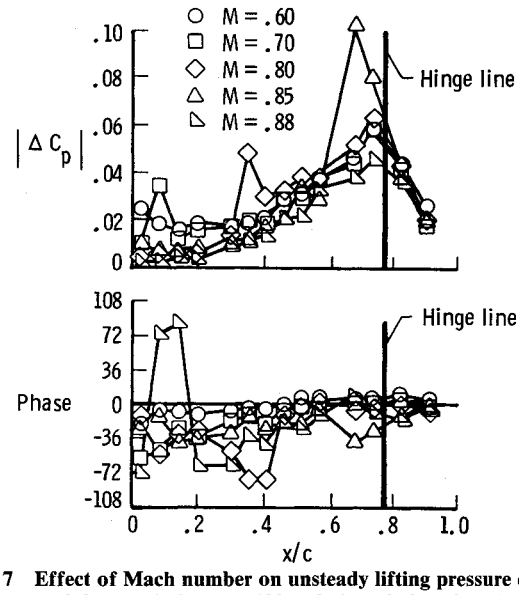

Fig. 7 Effect of Mach number on unsteady lifting pressure distribution at $\eta=0.87$; $\alpha=2$ deg, $q=100$ psf, $\delta_m=0$ deg, $\delta_d=1$ deg, and $f=15$ Hz.

surface deflection δ_m of 0 deg. As Mach number increases, a shock can be seen to have formed near 30% chord at a Mach number equal to 0.80 and to move aft to about 70% chord at a Mach number equal to 0.88. Attached flow is indicated at all Mach numbers except at a Mach number of 0.88, where the pressure distribution indicates flow separation on the upper surface near the trailing edge.

Angle-of-Attack Effects

The variation of the steady lifting pressure with angle of attack at Mach number 0.80 and dynamic pressure of 100 psf is shown in Fig. 6 for the 87% span station. The shock develops and moves aft as the angle of attack increases from -2 to 4 deg.

Unsteady Pressure Results

Mach Number Effects

Figure 7 shows the variation of the unsteady lifting pressure distribution with Mach number at the 87% span station. The outboard control surface was oscillated with an amplitude $\delta_d=1$ deg about a mean deflection of $\delta_m=0$ deg at 15 Hz. The magnitude and phase components of the unsteady lifting pressure are plotted vs fraction of wing chord. For all Mach numbers, a peak in the pressure magnitude occurs just forward of the control surface hinge line location. An additional peak in the magnitude can be seen to occur at the mean shock

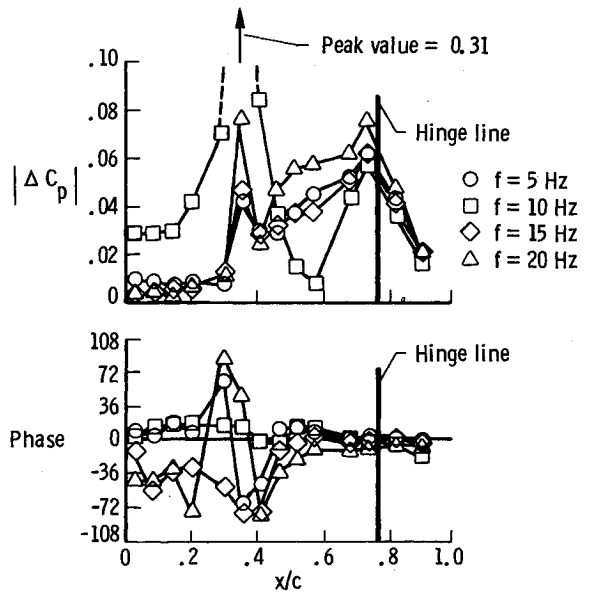

Fig. 8 Effect of frequency on unsteady lifting pressure distribution at $\eta = 0.87$; $M = 0.80$, $\alpha = 2$ deg, $q = 100$ psf, $\delta_m = 0$ deg, and $\delta_d = 1$ deg.

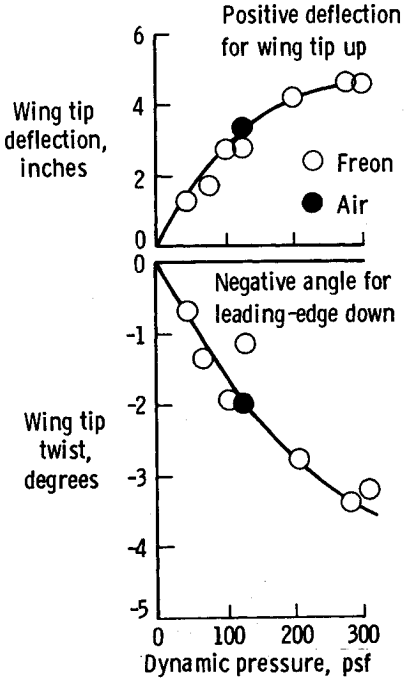

Fig. 9 Measured static wing-tip deflections vs dynamic pressure; $M = 0.80$ and $\alpha = 0$ deg.

location, as shown in Fig. 5 for Mach numbers 0.70–0.85. This peak is probably caused by the shock motion generated by the oscillatory control surface motion. The mean shock location can be seen to move aft with increasing Mach number. The mean shock peak and control hinge line peak appear to merge at a Mach number of 0.85. The peak in the pressure magnitude near the control surface hinge line increases with increasing Mach number through 0.85 but then drops to the lowest value at a Mach number of 0.88. In addition, no mean shock peak can be seen in the pressure magnitude at a Mach number of 0.88. These phenomena may be attributable either to the flow separation that occurs in the trailing-edge region of the wing at

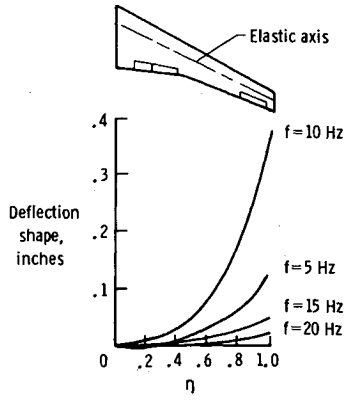

Fig. 10 Effect of frequency on wing amplitude at elastic axis; $M = 0.80$, $\alpha = 2$ deg, $q = 100$ psf, $\delta_m = 0$ deg, and $\delta_d = 1$ deg.

a Mach number of 0.88 or to the transducers being too far apart near the hinge line to show the existence of a peak.

Frequency Effects

Figure 8 shows the variation of the unsteady lifting pressure with the control surface oscillation frequency at the 87% span station. At the upper surface mean shock location, the magnitude of the unsteady pressure increases with increasing frequency from 5 to 20 Hz, except at 10 Hz. The magnitude peak for the 10-Hz oscillation is much greater than that for the other frequencies, probably because this 10-Hz frequency was very close to the wing first bending frequency of 8.3 Hz (wind-off).

Wing Deflections

For rigid wing pressure studies, the assumption is made that the wing does not deform, and therefore only the measured pressure distributions are needed. In contrast, for pressure studies on elastic wings, as in this study, the above assumption is not true. Therefore, both the measured pressure distributions and the corresponding measured deformed wing shape are needed to define the aerodynamic loading characteristics for a given wing configuration.

In the present study, a technique known as stereophotogrammetry was used to measure the static wing deflections.[9] Owing to the large amount of labor required to read the photos and analyze the data, the stereophotogrammetry deflection results are not available at this time. However, during these tests, some deflection measurements of the wing tip were made using a cathetometer instrument focused on a straight line drawn on the tip of the wing. Both vertical deflections and angular deflections of the wing tip were measured at selected test points. Illustrative results of these wing-tip deflection measurements at a Mach number of 0.80 and an angle of attack of 0 deg are shown in Fig. 9. The variation of the wing-tip vertical deflection with dynamic pressure is presented in Fig. 9, along with the associated wing-tip twist angle. Clearly, the elastic wing exhibits significant nonlinear tip deflections, with vertical deflections of over 4 in. and a negative tip twist of over 3 deg occurring at the higher dynamic pressures.

The present study used selectively spaced accelerometers mounted on the wing to obtain dynamic wing deflections for all wing tests of forced oscillatory motion. A discrete Fourier analysis was performed on each accelerometer signal at the known frequency of oscillation to obtain the amplitude of acceleration, which was then integrated twice to obtain magnitude of the motion at the corresponding wing location.

Figure 10 shows the wing delection mode shape derived from the accelerometer data for the cases shown in Fig. 8. The vertical deflection at the elastic axis is plotted for four oscillation frequencies. The elastic axis is located midway between the accelerometers shown in Fig. 2. As mentioned, at excita-

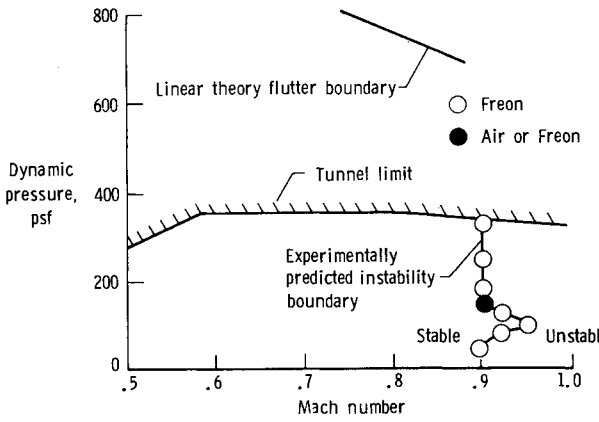

Fig. 11 Experimental and linear theory predictions of wing instability boundary.

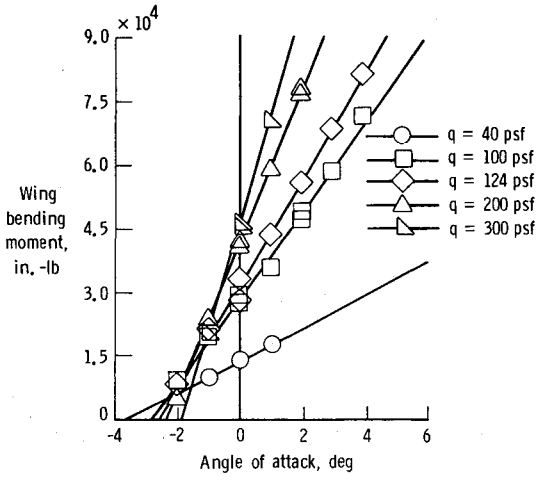

Fig. 12 Wing bending moment variation with angle of attack at five dynamic pressures; $M=0.80$ and $\delta_m=0$ deg.

tion frequencies near 10 Hz, the coupling of the forcing function frequency with the wing's first bending mode caused large dynamic wing deflections. Testing at 10 Hz was therefore discontinued after tests at only a few wing and tunnel conditions.

Wing Instability

An unusual wing instability, similar to wing first bending motion, was encountered at the beginning of these tests. The occurrence of the instability was surprising at the low dynamic pressures of about 100 psf where it was first encountered at a Mach number of about 0.90. This instability generated much interest as to its character, and the boundary was determined for a wing angle of attack and control surface deflection of 0 deg within the wind-tunnel limits, as shown in Fig. 11. Also shown in Fig. 11 as a solid line is the predicted linear theory (doublet-lattice) flutter boundary for comparison with the much lower dynamic pressures of the measured instability boundary. The experimentally predicted boundary was determined using a familiar subcritical response technique known as peak-hold.[10] Although the peak-hold results show a definite indication of instability onset, hard instability (zero damping) points were avoided for fear of damaging the model and thereby risking both the unsteady pressure tests and the DAST flight test program. An exception to this policy was the very lowest dynamic pressure point on the boundary, where a sustained limit amplitude oscillation was obtained at a Mach number of 0.895, and with a slight increase in Mach number to 0.900 the wing became stable. This exercise was performed to establish that the test conditions at this point were at or near

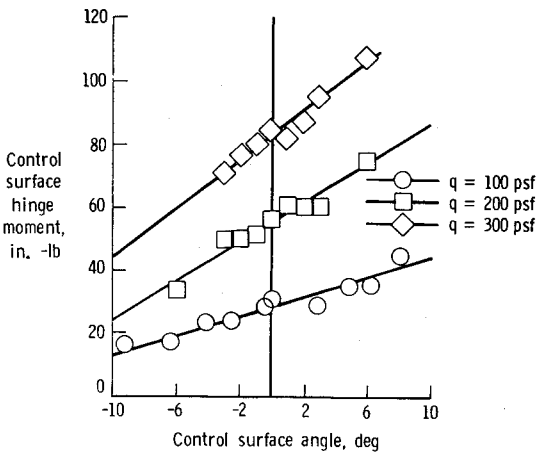

Fig. 13 Control surface hinge moment variation with control surface deflection at three dynamic pressures; $M=0.80$ and $\alpha=0$ deg.

the boundary minimum. The boundary occurs at a nearly constant Mach number of 0.90, beginning at a low dynamic pressure of about 50 psf and rising almost vertically to over 300 psf. At this time, no adequate explanation can be given for the higher Mach number variation in the boundary near 100 psf. The observed wing motion during the instability was similar to the wing first bending mode, the frequency of which was measured to be 8.3 Hz in the wind-off model vibration tests. The instability frequency was 8.6 Hz at the lowest dynamic pressure point and increased with dynamic pressure to about 13 Hz at the highest dynamic pressure point. It is interesting to note that the predicted flutter frequency was 24.3 Hz at a Mach number of 0.80.

Because of much recent interest in angle-of-attack effects and shock-induced effects on wing instabilities,[11-13] several additional tests were made that included variation of the wing angle of attack as the boundary was approached, comparison of air and Freon instability boundaries, and comparison of the boundaries with and without a transition strip near the wing leading edge. The instability was found to be sensitive to variation in angle of attack and, generally, the minimum damping occurred at or near zero angle of attack. In Fig. 11, the solid symbol indicates the Mach number and dynamic pressure at which the comparison tests were made. The results showed no significant difference in the instability boundary for tests in air or Freon. There were also no significant differences for tests in Freon with or without a transition strip.

Wing Bending Moments

Static wing bending moments were measured for a wide variety of conditions. For a given Mach number and dynamic pressure, the wing bending moments were measured as the wing angle of attack was varied from -2 to 4 deg. The result of these measurements for a Mach number of 0.80 is shown in Fig. 12, where the bending moment variation with wing angle of attack is shown for several values of dynamic pressure. The bending moments essentially vary linearly with angle of attack but are not linear with variations in dynamic pressure. This nonlinearity is due to the loss of lift at the wing tip resulting from the negative tip twist that occurred with increasing dyamic pressure, as shown in Fig. 9. The bending moment shows essentially no variation with dynamic pressure near -2.0 deg angle of attack.

Control Surface Hinge Moments

Measured static control surface hinge moments for a Mach number of 0.80 and zero angle of attack are presented in Fig. 13. The results are shown in terms of hinge moment variation with control surface angle for several values of dynamic pressure. The overall results appear to be reasonably linear over the range of test parameters although some scatter in the data can be observed.

Concluding Remarks

Steady and unsteady pressures were measured on an elastic high-aspect-ratio supercritical wing. An outboard trailing-edge control surface was oscillated at various amplitudes and frequencies to obtain unsteady data. The data were acquired for a wide range of test conditions, which included variations in Mach number from 0.60 to 0.90, dynamic pressure from less than 50 to over 300 psf, wing angle of attack from -2 to 4 deg, control surface mean angle from -8 to 8 deg, and control surface oscillation amplitudes of 1, 2, and 3 deg at frequencies of 5, 10, 15, and 20 Hz. Static and dynamic wing deflections were also measured. In addition, static wing bending moments and static control surface hinge moments were measured.

A subcritical response technique was used to predict experimentally an unusual dynamic wing instability boundary at much lower dynamic pressure values than those of the theoretically predicted flutter boundary. This wing instability boundary was well defined and occurred at a nearly constant Mach number of about 0.90 and varied in dynamic pressure from below 50 psf to above 300 psf. The frequency of this wing instability ranged from about 8.6 Hz at the minimum dynamic pressure to about 13 Hz at the maximum dynamic pressure. The wing instability motion was dominated by the wing first bending mode, which had a measured frequency of 8.3 Hz during the ground vibration tests. The instability was found to be sensitive to angle of attack, with minimum damping occurring near zero degrees. Comparison tests conducted in air and Freon showed no significant difference in the instability boundary. Tests in Freon with and without a transition strip also showed no significant differences.

References

[1]Hess, R. W., Wynne, E. C., and Cazier, F. W. Jr., "Static and Unsteady Pressure Measurements on a 50 Degree Clipped Delta Wing at $M=0.9$," NASA TM-83297, April 1982.

[2]Sandford, M. C., Ricketts, R. H., Cazier, F. W. Jr., and Cunningham, H. J., "Transonic Unsteady Airloads on an Energy Efficient Transport Wing with Oscillating Control Surfaces," *Journal of Aircraft,* Vol. 18, July 1981, pp. 557–561.

[3]Ricketts, R. H., Sandford, M. C., Seidel, D. A., and Watson, J. J., "Transonic Pressure Distributions on a Rectangular Supercritical Wing Oscillating in Pitch," *Journal of Aircraft,* Vol. 21, Aug. 1984, pp. 576–582.

[4]Murrow, H. N. and Eckstrom, C. V., "Drones for Aerodynamic and Structural Testing (DAST)—A Status Report," *Journal of Aircraft,* Vol. 16, Aug. 1979, pp. 521–526.

[5]Eckstrom, C. V., "Loads Calibration of Strain Gage Bridges on the DAST Project Aeroelastic Research Wing (ARW-2)," NASA TM-87677, March 1986.

[6]Byrdsong, T. A. and Cuyler, W. B. Jr., "Wind-Tunnel Investigation of Longitudinal and Lateral-Directional Stability and Control Characteristics of a 0.237-Scale Model of a Remotely Piloted Research Vehicle With a Thick, High-Aspect-Ratio Supercritical Wing," NASA TM-81790, July 1980.

[7]Cole, P. H., "Wind Tunnel Real-Time Data Acquisition System," NASA TM-80081, April 1979.

[8]Chapin, W. G., "Dynamic-Pressure Measurements Using an Electronically Scanned Pressure Module," NASA TM-84650, July 1983.

[9]Brooks, J. D. and Beamish, J. K., "Measurement of Model Aeroelastic Deformations in the Wind Tunnel at Transonic Speeds Using Stereophotogrammetry," NASA TP-1010, Oct. 1977.

[10]Sandford, M. C., Abel, I., and Gray, D. L., "Development and Demonstration of a Flutter-Suppression System Using Active Controls," NASA TR-R-450, Dec. 1975.

[11]Yates, E. C. Jr., Wynne, E. C., and Farmer, M. G., "Effects of Angle of Attack on Transonic Flutter of a Supercritical Wing," *Journal of Aircraft,* Vol. 20, Oct. 1983, pp. 841–847.

[12]Persoon, A. J., Horsten, J. J., and Meijer, J. J., "Measurement of Transonic Dips in the Flutter Boundaries of a Supercritical Wing in a Wind Tunnel," *Journal of Aircraft,* Vol. 21, Nov. 1984, pp. 906–912.

[13]Dobbs, S. K., Miller, G. D., and Stevenson, J. R., "Self-Induced Oscillation Wind Tunnel Test of a Variable Sweep Wing," AIAA Paper 85-0739, April 1985.